coatings

MDPI

Article

Study on Anti-Scale and Anti-Corrosion of Polydopamine Coating on Metal Surface

Xu-Liang Yu [1], Bing-Bing Wang [1,2,3,*], Zhi-Ming Xu [1] and Wei-Mon Yan [4,*]

[1] School of Energy and Power Engineering, Northeast Electric Power University, Jilin 132012, China
[2] School of Mechanical and Electrical Engineering, Chongqing Institute of Science and Technology, Qingcheng 332020, China
[3] Intelligent Manufacturing and Photoelectric Instrument Laboratory, Shenzhen Research Institute, Beijing Institute of Technology, Shenzhen 518057, China
[4] Department of Energy and Refrigerating Air-Conditioning Engineering, National Taipei University of Technology, Taipei 10608, Taiwan
* Correspondence: wangbb@neepu.edu.cn (B.-B.W.); wmyan@ntut.edu.tw (W.-M.Y.); Tel.: +86-0432-64807281 (B.-B.W.); +886-972015310 (W.-M.Y.)

Abstract: Some surface coatings can protect metal surfaces and reduce scale deposition. Based on that, the biomimetic material polydopamine (PDA) can form a stable coating on many material surfaces; therefore, we propose an efficient one-step electroplating method for preparing anti-scale PDA coatings with high stability. The scale deposition test showed that the deposition weight of calcium carbonate on the coating is less than that of carbon steel after immersing in a supersaturated solution of calcium carbonate for 12 h at 70 °C and 90 °C, with a coating scale-inhibition efficiency of 55.02% and 66.96%, respectively. By using molecular dynamics simulation, it was found that water adsorption layers exist near the metal's surface, and the existence of water adsorption layers on the hydrophilic surface is the main reason for the initial deposition of calcium carbonate. The interaction energy between the PDA molecular layer and water is weaker (−5.69 eV) for the surface with the PDA coating, and there is no dense water adsorption layer on the coating, which leads to the low probability of calcium carbonate adsorption on the PDA coating surface. Therefore, PDA coating can inhibit the deposition of calcium carbonate on the surface.

Keywords: PDA coating; electroplating; stability; corrosion resistance; scale inhibition; molecular dynamics simulation

Citation: Yu, X.-L.; Wang, B.-B.; Xu, Z.-M.; Yan, W.-M. Study on Anti-Scale and Anti-Corrosion of Polydopamine Coating on Metal Surface. *Coatings* **2023**, *13*, 306. https://doi.org/10.3390/coatings13020306

Academic Editors: Devis Bellucci and Alina Vladescu

Received: 22 December 2022
Revised: 18 January 2023
Accepted: 19 January 2023
Published: 29 January 2023

1. Introduction

Scale is a layer of solid or oozy material that gradually accumulates on a solid surface in contact with a fluid. Scale deposition on the surface of pipes and heat exchange equipment is a widespread problem in various industrial fields, which not only leads to the reduction in heat exchange efficiency but results in the corrosion of the equipment's surface, thus causing huge security risks and economic loss [1–5]. In order to reduce the formation and attachment of scale on the surface of equipment, researchers have developed many anti-scale methods, such as scale inhibitors, electric field anti-scale, etc., [6–10], but effective anti-scale measures are still very limited. The application of these scale-inhibition and descaling methods causes a series of problems, such as a large amount of water pollution, equipment corrosion, and high cost. Under the pressure of increasing water shortage and sustainable environmental development, the use of these methods will be gradually limited or even eliminated. As another modification method of the solid surface, anti-scale coating can reduce the adhesion strength between the scale and heat transfer interface, reducing the deposition of scale. The coating can also effectively isolate the plate from the outside world and prevent external damage to the base material [11,12].

Polydopamine (PDA) coating can be formed on the surface of any material, and has the advantages of wide applicability, strong binding force, good flexibility, etc., [13]. It is worth noting that the PDA coating has excellent corrosion resistance [14]. At present, PDA composite coating is mostly used in scale inhibition [1,15–17], in which PDA mainly plays the role of adhesion and fixation; however, whether PDA coating itself has a scale-inhibition effect is not yet clear. In the traditional chemical preparation process of PDA coating, dopamine polymerization must be induced by adding oxidizer to neutral or acidic water media [18–20]. In addition, the preparation process of PDA will be affected by many factors, such as pH, temperature, reaction time, and so on [21]. For example, Wang et al. [1] calibrated the configured Tris buffer pH value as 8.5, mixed it with dopamine solution, then added ammonium persulfate oxidant, and immersed the base in the reaction solution at 50 °C for 6 h to prepare PDA coating. Tris buffer or oxidant components will inevitably be doped into the coating, which may change the physicochemical properties of the coating [21,22].

The electroplating process has many advantages, such as a simple preparation method, low cost, controllable plating conditions, and unlimited base size [23–25]. It was found that plating accelerated the dopamine polymerization rate and facilitated the preparation of PDA coating [26–28]. For example, Xiang et al. [28] used dopamine, nickel sulfate, copper sulfate, sodium sulfate, and n-dodecanethiol as electrolytes to successfully prepare super hydrophobic and super oil-philic coating on stainless steel mesh by electroplating.

In many industrial applications, such as water treatment, heat exchanging, etc., the formation of calcium carbonate ($CaCO_3$) scales on the surface of a pipe or equipment is a critical concern. This work proposes to prepare the PDA coating on the metal surface, obtain the $CaCO_3$ scale-suppression properties, and explore the microscopic mechanism of scale inhibition by molecular dynamics simulation. Ni is widely recognized as the most widely used surface finishing material, with excellent corrosion resistance, and Ni^{2+} can be used as a polymeric oxidant of dopamine [26–28]. In the preparation, the dopamine aqueous solution is used as the electrolyte, and the high-purity Ni plate (Ni 99.99%) is used as the anode. During the electroplating process, the anode releases Ni^{2+}, and the Ni^{2+} drives the dopamine to move to the cathode metal substrate. Meanwhile, dopamine promoted the electrodeposition of Ni^{2+}. The proposed one-step plating method yields stable PDA coatings on a variety of metal surfaces in only a few minutes. The coating performance test shows that the prepared PDA coating has excellent stability, corrosion resistance, and scale-suppression properties.

Molecular dynamics simulations can explore the mechanism of the inhibition of $CaCO_3$ adsorption by the scale-inhibitor mechanism from a microscopic perspective [7]. The initial formation of $CaCO_3$ scale is the adsorption behavior of $CaCO_3$ ions on the surface. In this paper, stable PDA coatings were first prepared on metal surfaces by simple and efficient one-step electroplating methods. Additionally, after serial characterization, the inhibition of $CaCO_3$ crystalline scale by PDA coating was evaluated by the weighing method. The adsorption and interaction energy of $CaCO_3$ on the surface with or without coating was obtained by the molecular dynamics simulation method, and the mechanism of inhibiting the formation of calcium carbonate scale by PDA coating was qualitatively revealed from the molecular point of view.

2. Experimental Section

2.1. Materials

The substrate used in the study was Q235 carbon steel. Dopamine hydrochloride (DA, 98%, MW = 189.64 g/mol) was purchased from Sigma-Aldrich Corporation (St. Louis, MO, USA). All experiments were performed with deionized water. All reagents are analytical grade and require no further purification.

2.2. Fabrication of PDA Coating

This preparation method can successfully prepare PDA coating on the surface of conductive metal substrate, and PDA coating has been successfully prepared on the surface of carbon steel, stainless steel, and copper metal. Here, carbon steel is selected as the substrate for coating preparation and properties. First, the 0.5 mm thick Q235 carbon steel plate was laser cut into a 30 × 10 mm^2 test plate, and then ground by SiC sandpaper with a mesh size of 280–1000 in sequence. Prior to experiment, the sample was ultrasonically treated with acetone, ethanol, and DI water. The plating solution was 1.2 g/L of dopamine solution without the addition of other reagents. The plating process was carried out in a double-electrode electrochemical reaction tank, using Ni 99.99% high-purity nickel plate as anode, pretreatment Q235 carbon steel as cathode, and the spacing between the two-electrode plates fixed at 20 mm. During plating, the voltage control was 15 V, and the temperature was kept at about 35 °C. After 3 min of electroplating, the cathode samples were removed from the plating solution and dried in 25 °C air.

The principle of PDA coating preparation is shown in Figure 1. Driven by an electric field, the anode releases the Ni^{2+}, and the Ni^{2+} drives the dopamine to move towards the cathode metal surface. Ni^{2+} accelerates the polymerization rate of dopamine on the cathode metal substrate surface; meanwhile, dopamine promotes the deposition of Ni on the cathode surface. Therefore, the one-step electroplating method can form a stable PDA coating on the metal surface within a few minutes.

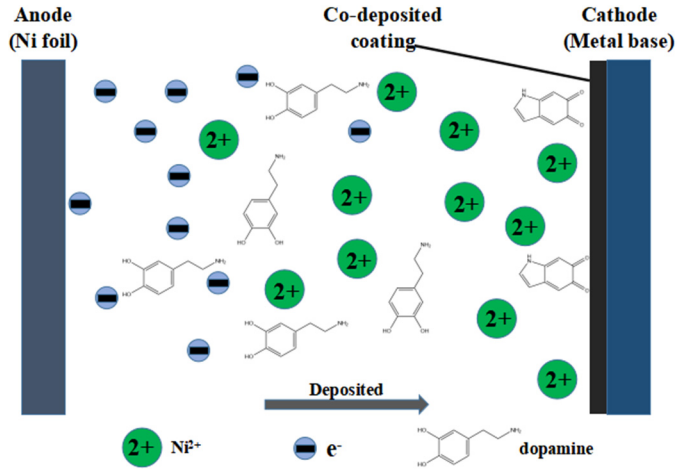

Figure 1. Schematic diagram for fabrication of PDA coating by one-step electrodeposition.

2.3. Surface Characterization

The surface morphology of the coating was analyzed by focusing ion field-emission scanning electron microscopy (FIB-SEM, Crossbeam 350, Carl Zeiss AG, Oberkochen, Germany), and the surface chemical composition of the sample was detected by energy-dispersive spectroscopy (EDS, OXFORD INSTRUMENTS, Oxford, UK). The static contact angle of the sample surface was determined by SDS-200 contact Angle tester (SINDIN, Dongguan, China) using the droplet method. The droplets measured were 3 μL, and the average contact angle was obtained by measuring three locations of a sample. The stability of the coating is very important in practical application. Therefore, the adhesive properties between the coating and Q235 carbon steel substrate were firstly tested by the tape stripping method in this study. The tape stripping test is as follows: place the sample on the horizontal table, the surface of the sample is compacted and completely covered with tape, and then the entire tape is slowly stripped.

Corrosion degradation of metal materials is an electrochemical corrosion process, which can be analyzed by electrochemistry. CHI660e electrochemical workstation (Shanghai Chenhua Instrument Co., LTD., Shanghai, China) was used for the electrochemical test of the sample. A three-electrode system was adopted, with the sample to be tested as

the working electrode, the platinum electrode as the auxiliary electrode, the saturated glymeromal electrode (SCE) as the reference electrode, and 3.5 wt.% NaCl solution as the corrosive solution. The polarization curve (PC) of the samples was measured, with a scanning potential range from −1.0 to −0.2 V, and the scanning rate was 1 mV/s. A total of 1 cm^2 of the working electrode is exposed as the working face, and the rest part is sealed with paraffin wax. Each electrode was placed in the electrolyte and connected to an electrochemical workstation. After hardware test, the open-circuit potential was detected. When the potential value stabilized (about 15 min), the polarization curve was measured.

3. Molecular Dynamics Calculations

3.1. Model Construction

In this work, we simulated the adsorption process of calcium carbonate in metal plates by using Materials Studio software (version 19.1.0.2353). As shown in Figure 2, the initial model is a cuboid box, and Figure 2a is an Fe plate box model with a size of 27.8 × 27.8 × 80.1 $Å^3$, with a plate area, a solution area, and a vacuum area from bottom to top. Figure 2b shows a box model containing the PDA molecules. The size is 27.8 × 27.8 × 94.2 $Å^3$, with a 6.5 Å thick PDA polymer region added in the middle. Here, to avoid periodic boundary conditions, a vacuum layer with 20 Å thickness is added along the system's Z direction. Among them, the plate contains 621 Fe atoms with a thickness of 8.599 Å, a cubic lattice structure, and a lattice constant of 2.8664 Å.

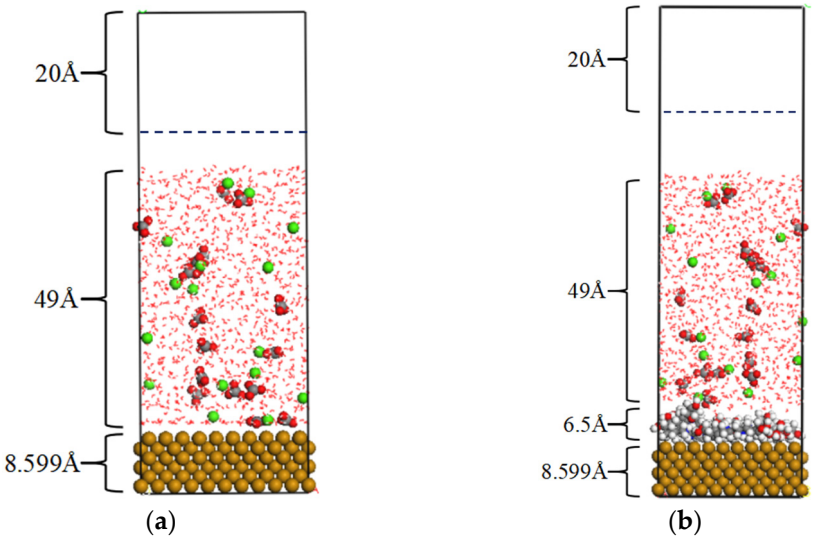

Figure 2. Initial simulation system: (**a**) Fe plate and (**b**) Fe plate with PDA coating.

The total simulation time was 4000 ps, with a simulation time step of 1 fs. The CAMPASS force field was used for simulation [29–32], and the simulation system was an NVT ensemble. Ewald- and atom-based summation methods were used to calculate the electrostatic and van der Waals interactions between atoms for non-bond interactions. The cutoff radius was chosen at 12.5 Å.

3.2. Equilibrium Judgment of Simulated System

The fluctuation curves of energy and temperature are usually used to determine the equilibrium of the system. When the fluctuation range of energy and temperature curves is within 5%–10%, the equilibrium of the system has been achieved [7]. The energy and temperature curves of the simulation system with or without PDA coating (Figure 2a,b) are shown in Figure 3. Within 1000 ps after the equilibrium stage, the temperature and energy of the system fluctuated very little, which is within the uncertainty of 5%–10%. Therefore, it indicates that the energy and temperature of the simulation system have reached the equilibration phase, further confirming the reliability of using 1000 ps during

the equilibrium phase to carry out the result analysis, indicating that the system reached the equilibrium state.

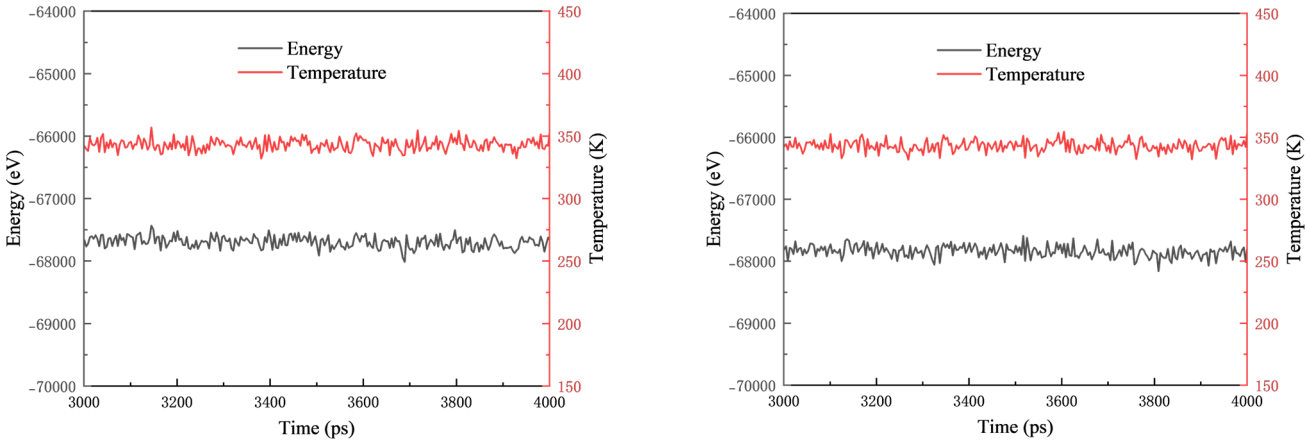

Figure 3. Evolution of system temperature and energy for (**a**) Fe plate and (**b**) PDA coating.

4. Results and Discussion

4.1. Experimental Section

4.1.1. Surface Morphology and Coating Composition

Figure 4a shows a macroscopic image of the coating of carbon steel prepared with a one-step electroplating process. The prepared coating appears uniformly dark brown. Figure 4b shows the SEM image of the surface morphology of the coating. It can be seen that the carbon steel surface is a "coral-like" cluster structure composed of nanoscale spheres, with cluster diameters ranging from 50 to 200 nm. The chemical composition of the sample surface was detected by the EDS spectral analyzer, as shown in Figure 4c,d. Elements Ni, C, N, and O exist in the prepared coating, and all elements are evenly distributed on the surface of the substrate (Figure 4d), where C, N, and O are the main component elements of PDA. The results show that the prepared coating is a PDA coating with nanostructures.

4.1.2. Coating Stability

In practical applications, coating stability is critical for preserving surface function and durability. The tape stripping method was used to test the coating stability [33]. Figure 5 shows the change in the water contact angle on the surface of the PDA coating after different strip times. The static water contact angle of the sample surface was measured by a contact-angle-measuring instrument. The contact angle of water on the surface of carbon steel is 72.01 $\pm$ 0.3°, and the contact angle of water on the surface of the PDA coating is 60.45 $\pm$ 0.3°. If the coating is glued away during the tape stripping test, the contact angle will rise markedly. After performing tape stripping experiments 50 times, the water contact angle on the surface of the sample slightly increased from 60.45 $\pm$ 0.3° to 62.22 $\pm$ 1°. In the subsequent 150 times of tape stripping experiments, the water contact angle was 62.69 $\pm$ 0.3°, and the contact angle only increased by 0.47°. The coating prepared by electrodeposition consists of two parts: physical adsorption and stable adsorption. During the first 50 tape stripping experiments, the physical adsorption part was stripped off by the tape, so the contact angle changed. The remaining stable adsorption part can hardly be removed by the tape, so the contact angle changes little after 150 times. The tape experiment shows that the PDA coating has good stability on the carbon steel substrate.

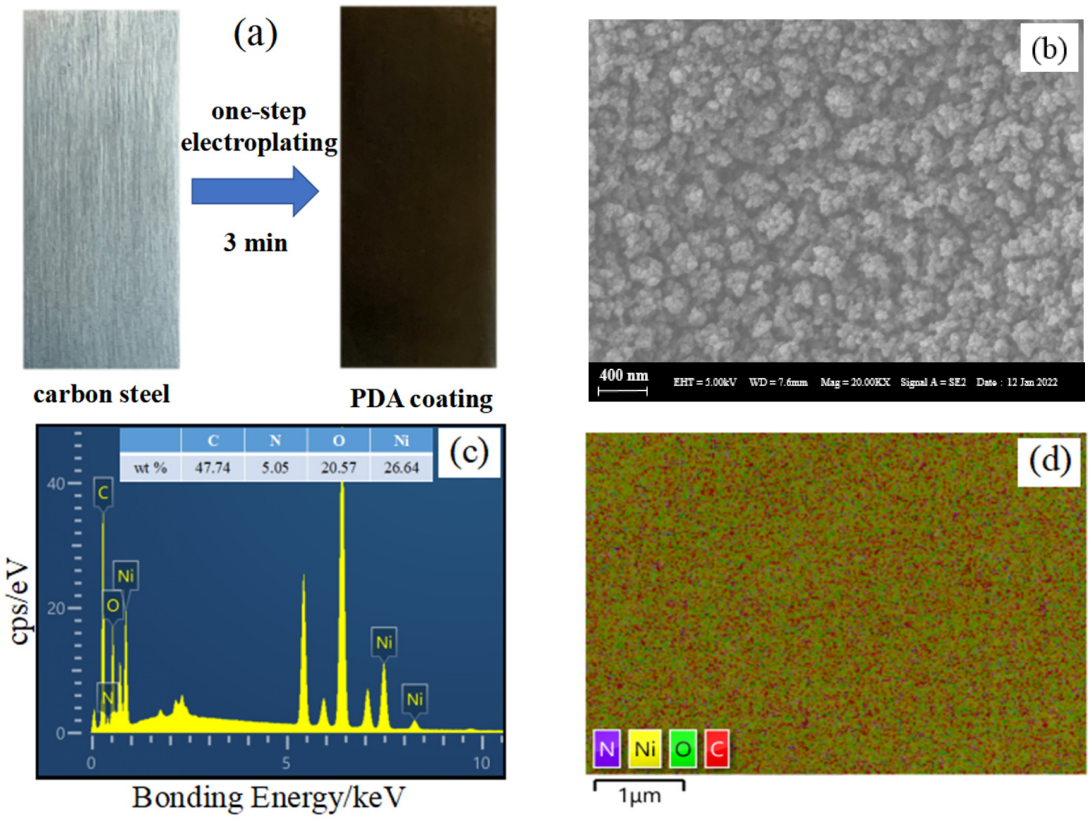

Figure 4. (**a**) Image of carbon steel and PDA-Ni coating, and (**b**) SEM-, (**c**) EDS-, and (**d**) EDS-layered image for PDA coating.

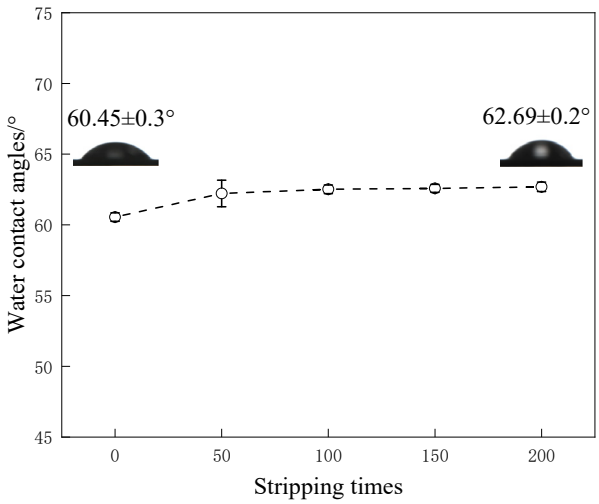

Figure 5. Evolution of water contact angle of PDA coating vs. stripping times.

4.1.3. Anti-Corrosion Performance

The electrochemical methods were used to study the electrochemical corrosion characteristics of different samples after soaking in 3.5 wt.% NaCl solution for 24 h. The potentiodynamic polarization curves of carbon steel and PDA coating are shown in Figure 6. The electrochemical method has the advantages of fast measurement speed and a short experiment period. The corrosion parameters of carbon steel (CS) and PDA coating obtained by potentiodynamic polarization curves are listed in Table 1 [23,34,35]. A positive corrosion potential (E_{corr}) represents a lower thermodynamic corrosion trend, and a smaller corrosion current density (J_{corr}) represents a lower corrosion kinetic rate.

Therefore, the more positive the corrosion potential and the smaller the corrosion current density, the better the corrosion-inhibition performance of the coating [36]. Compared with Q235 carbon steel, the modified surface with PDA coating has lower corrosion current density and higher corrosion potential. The corrosion current density is 8.534 μA·cm^{-2}, which is about 1/9 of the carbon steel substrate. Usually, the polarization resistance (R_p) is also one of the parameters that reflect the degree of corrosion resistance of the material. The polarization resistance R_p is calculated by the following formula:

$$R_p = \frac{b_a \times |b_c|}{2.303 \times (b_a + |b_c|) \times J_{corr}} \quad (1)$$

where R_p is the polarization resistance, J_{corr} is the self-corrosion current density, and b_a and b_c are the Tafel slope of anode and cathode, respectively. In general, the greater the R_p, the less likely the material is to corrode. As can be seen from Table 1, the R_p of PDA coating is seven times more in comparison with that of the Q235 carbon steel substrate.

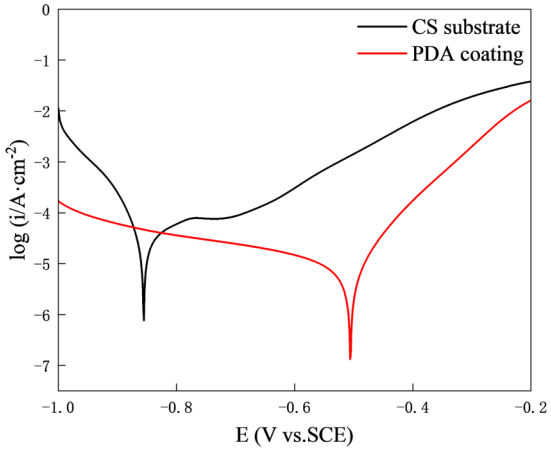

Figure 6. Potentiodynamic polarization curves of carbon steel (CS) and PDA coating in 3.5 wt.% NaCl solution.

Table 1. Corrosion parameters of carbon steel (CS) and PDA coating obtained by potentiodynamic polarization curves.

Samples	E_{corr}/V	J_{corr}/μA·cm^{-2}	η/%	R_p/kΩ · cm^{-2}
CS	−0.855	74.62	-	0.466
PDA coating	−0.506	8.534	88.56%	3.262

The corrosion-suppression efficiency η is defined as [37]:

$$\eta = \left[\left(J^0_{corr} - J_{corr}\right) / J^0_{corr}\right] \times 100\% \quad (2)$$

where η is the corrosion-inhibition efficiency, and J^0_{corr} and J_{corr} are the self-corrosion current density of Q235 carbon steel and PDA coating, respectively. The inhibition efficiency of PDA coating on the Q235 carbon steel is 88.56%.

4.1.4. Anti-Scale Performance

The inhibition of calcium carbonate crystalline scale by PDA coating was evaluated by weighing method. The test solution was calcium carbonate supersaturated, and the concentrations of Ca^{2+} and CO_3^{2-} were 360 mg/L. The carbon steel and PDA coating samples were statically immersed in calcium-carbonate-saturated solution for 12 h and

then naturally dried at ambient temperature. Formula (3) was used to calculate the scale deposition per unit area [23].

$$W_{\text{per area}} = \frac{W_S - W_0}{A} \quad (3)$$

where W_0 and W_s are the quality of the samples before and after the experiment, respectively, and A is the surface area of the sample. Response surface methodology using ANOVA can be useful for better data evaluation and model development [38]. This is a topic for future work.

Figure 7 shows the amount of scale deposition of carbon steel and PDA coating after being immersed in calcium carbonate solution at 70 °C and 90 °C for 12 h. The amount of $CaCO_3$ scale deposition on the carbon steel surface is 0.667 and 0.672 mg/cm^2, respectively. For the PDA coating surface, the amount of calcium carbonate scale is 0.300 and 0.222 mg/cm^2, respectively, and the corresponding anti-scale rates of the coating are 55.02% and 66.96%, respectively. The results show that PDA coating has a higher scale-inhibition effect in high-temperature solution.

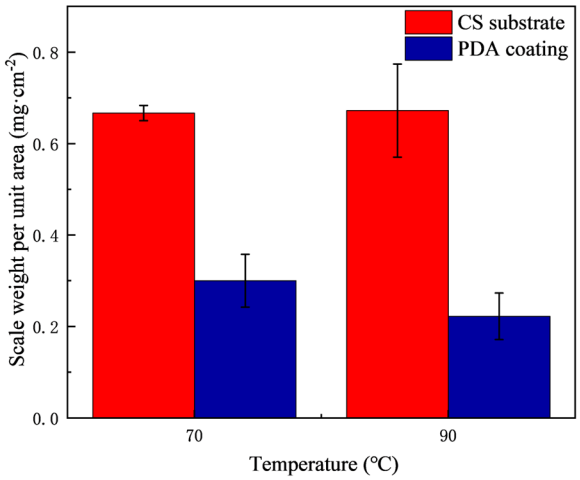

Figure 7. Comparison of $CaCO_3$ scale deposition on carbon steel (CS) and PDA coating surface.

4.2. Molecular Dynamics Simulations

4.2.1. Adsorption Configuration of $CaCO_3$

The adsorption configuration of $CaCO_3$ in 0.8 mol/L supersaturated solution for Fe plate with or without PDA coating at different times is displayed in Figure 8. At the initial moment, the ions are uniformly distributed in the solution. For uncoated plates, ions near the plate were preferentially adsorbed to the plate under van der Waals attraction. However, the ions in the bulk phase are far away from the plate, and there is a strong electrostatic attraction between Ca^{2+} and CO_3^{2-}. During the Brownian motion of ions, $CaCO_3$ clusters are formed (Figure 8a 1 ns). Subsequently, the $CaCO_3$ cluster underwent irregular Brownian motion, and when the cluster was close to the plate during the thermal motion of the cluster, the van der Waals attraction between the cluster and the Fe atom increased significantly, and finally the clusters adsorbed on the plate surface at 4 ns. For the PDA coating surface (Figure 8b), only a portion of $CaCO_3$ ions absorbed on the coating surface at 4 ns. The simulation results show that compared with the metal plate, it was found that the probability of scale adsorption of PDA coating was significantly reduced, while the PDA coating presents the scale-inhibition effect. The scale-inhibition mechanism of PDA coating is analyzed in detail in the following section.

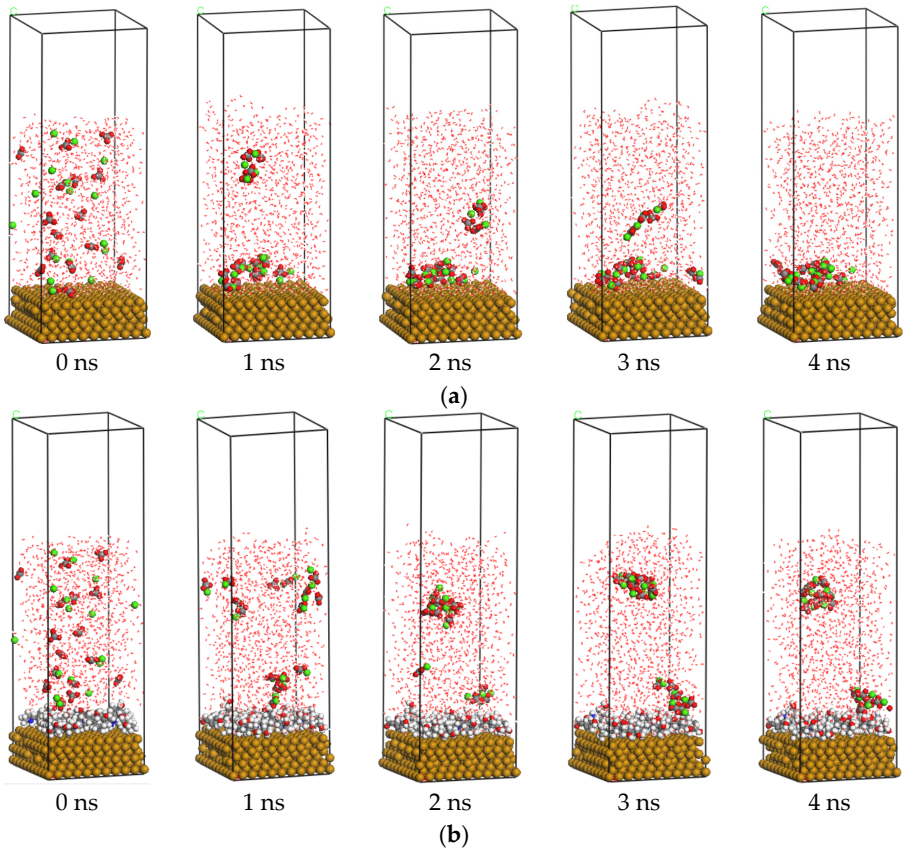

Figure 8. Adsorption configurations of $CaCO_3$ on (**a**) Fe plate and (**b**) PDA coating.

4.2.2. Water Molecular Adsorption Layer on the Surface

Figure 9 shows the number density of water molecules along the Z direction of the system at the initial moment (the deepened area in the figure is the plate). For an Fe plate without coating, the presence of two peaks near 2.9 Å and 5.9 Å from the surface represents two dense layers of water molecule adsorption distributed near the plate (as indicated in red and blue in the illustration). This is due to the strong van der Waals force between the Fe plate and nearby water molecules, and the thickness of the water adsorption layer is 6.9 Å at the second trough of the number density distribution. For the plate with PDA coating, there is no obvious peak of water molecular number density, indicating that a dense water molecule adsorption layer is not formed on the coating surface, which may be the reason why the PDA coating has an increased scale-inhibition performance.

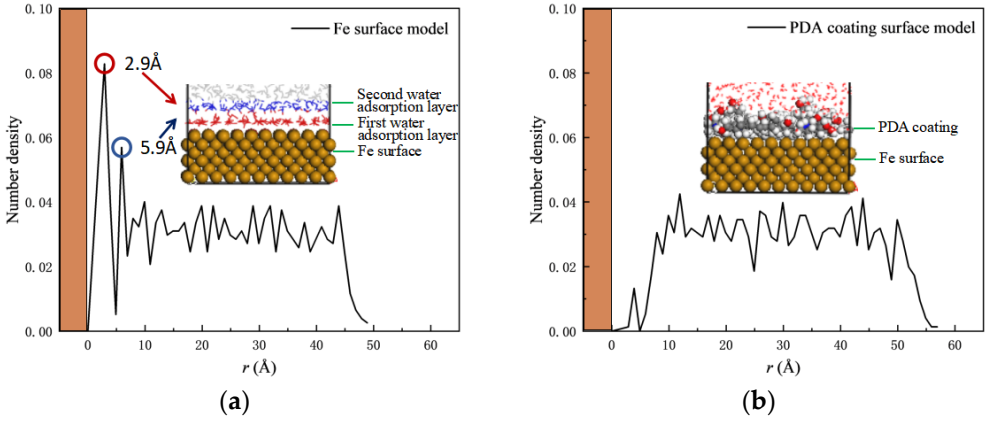

Figure 9. Number density distribution of water molecules oriented perpendicular to the surface. (**a**) Fe plate and (**b**) PDA coating, brown area is Fe plate.

In order to compare and analyze the water molecular adsorption layer near the Fe surface with or without PDA coating, the interaction energy $E_{interaction}$ calculation expression [39] is as follows:

$$E_{interaction} = E_{total} - (E_{surface} + E_1) \quad (4)$$

where $E_{interaction}$, $E_{surface}$, and E_1 represent the total energy of the computational system, the energy of the solid plate, and the energy of the water molecular within 6.9 Å, respectively. When $E_{interaction}$ is negative, it represents the attraction force, and the value of $E_{interaction}$ indicates the adsorption force of the plate to water molecular layers.

The interaction energies are listed in Table 2. It is calculated that the interaction energy between the Fe plate and the water molecular layer in 6.9 Å is −27.44 eV for the uncoated model. For the PDA coating model, the interaction energy between the plate (including the Fe plate and the PDA coating) and the water molecular layer is −7.51 eV. The adsorption force of the water molecular layer is much less for the uncoated Fe plate model. Therefore, the weak interaction between the PDA coating and water molecules leads to the absence of a dense water adsorption layer.

Table 2. Interaction energy of the surface with the water molecular layer within 6.9 Å.

Simulated Condition	E_{total}/eV	E_{Fe}/eV	E_{H_2O}/eV	$E_{interaction}$/eV
Fe surface (Fe-6.9 Å H_2O)	−2769.95	−2748.79	6.28	−27.44
PDA coating surface (plate-6.9 Å H_2O)	−2816.38	−2809.11	0.24	−7.51

4.2.3. Interaction between PDA Coating and $CaCO_3$

The adsorption strength can be expressed by the interaction energy [40]. In order to reveal the interaction between the PDA coating and $CaCO_3$, the interaction energy between $CaCO_3$ and the Fe plate with or without the PDA coating, as well as water adsorption layer at the initial moment, is calculated according to Equation (4), and the results are shown in Figure 10. For the Fe plate model, the interaction energy between the plate and $CaCO_3$ is −1.53 eV, and the interaction energy between the surface water adsorption layer and $CaCO_3$ is −84.22 eV, which is almost 55 times in comparison with the attraction energy between the Fe plate and $CaCO_3$. In addition, the interaction energy between the surface water adsorption layer and $CaCO_3$ is negative, indicating a strong attraction between the surface water adsorption layer and $CaCO_3$. Therefore, the presence of dense water adsorption layers is the main reason that leads to the adsorption behavior of $CaCO_3$ towards the Fe plate.

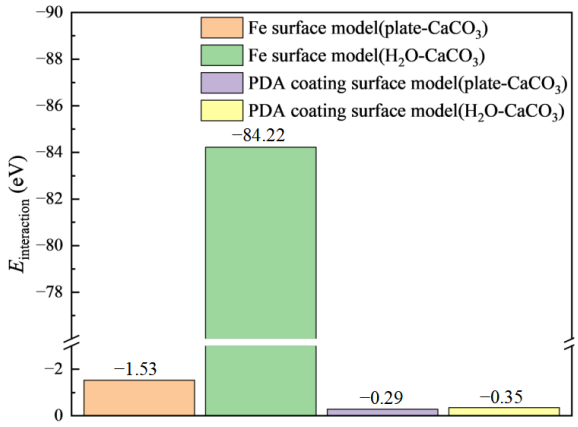

Figure 10. Comparison of interaction energy.

For the PDA-coated model, the interaction energies between the plate (including Fe plate and PDA coating) and $CaCO_3$, and the water molecular layer within 6.9 Å near

the coating surface and $CaCO_3$, are −0.29 eV and −0.35 eV, respectively. There is no dense water adsorption layer near the PDA coating surface, and it shows weak attraction to $CaCO_3$; therefore, PDA coating has the ability to inhibit $CaCO_3$ scale. As shown in Figure 8b, for the PDA coating model, although a small amount of calcium carbonate adsorbs on the plate, the interaction energy between the plate and the absorbed $CaCO_3$ cluster is only −1.85 eV, and the absorbed $CaCO_3$ can be easily removed from the PDA coating surface.

It was found that the dense water adsorption layer near the Fe surface is the main driving force of $CaCO_3$ scale formation by using MD simulations. The experiment test confirmed that PDA coating has the ability to inhibit $CaCO_3$ scale deposition. The anti-scale mechanism of PDA coating is that PDA molecules have a weak interaction with water molecules, and there is no dense water adsorption layer near the PDA coating surface; therefore, the adsorption probability of the $CaCO_3$ scale on the PDA surface reduces.

5. Conclusions

In this study, our proposed efficient one-step electroplating method can prepare stable PDA coating on the metal surface. By conducted an experimental test of the stability, corrosion resistance, and scale-inhibition performance of the PDA coating surface, and qualitatively revealing the anti-scale mechanism by molecular dynamics simulation, we found:

The water contact angle of the PDA coating surface changed by 2.24% after 200 tape stripping experiments, and the water contact angle demonstrated the excellent stability of the PDA coating. The corrosion-inhibition efficiency of PDA coating was 88.56%. The scale-inhibition test showed that the anti-scale rates of PDA coating were 55.02% and 66.96% after being immersed in the supersaturated solution of calcium carbonate at 70 °C and 90 °C for 12 h, respectively.

Dense water adsorption layers existed near the Fe plate, and there was a strong interaction energy (−84.22 eV) between the water adsorption layer and $CaCO_3$, which was the main driving force in the early stages of $CaCO_3$ scale deposition. There was a weak interaction between the PDA coating and water molecules, resulting in the absence of a dense water adsorption layer on the PDA coating surface, which reduced the adsorption probability of $CaCO_3$ on the PDA coating surface. Therefore, the PDA coating inhibited the $CaCO_3$ scale deposition.

Author Contributions: Methodology, X.-L.Y.; Investigation, X.-L.Y.; Writing—review & editing, Z.-M.X. and W.-M.Y.; Project administration, B.-B.W. All authors have read and agreed to the published version of the manuscript.

Funding: The authors would like to thank the National Natural Science Foundation of China (Grant No. 51976028), Science, Technology and Innovation Commission of Shenzhen Municipality (JCYJ2022053016480716), and the Education Department of Jilin Province (Grant No. JJKH20220102CY) for their support.

Institutional Review Board Statement: Not applicable.

Informed Consent Statement: Not applicable.

Data Availability Statement: Not applicable.

Conflicts of Interest: The authors declare no conflict of interest.

References

1. Wang, B.B.; Wang, X.; Xu, Z.M.; Zhao, Q.; Wang, X.D. Inhibition of adhesion of $CaCO_3$ scale by polydopa-mine/polytetrafluoroethylene coating with stability and anticorrosion properties. *J. Appl. Polym. Sci.* **2022**, *139*, e52066. [CrossRef]
2. Xu, Z.; Wang, J.; Han, Z.; Zhao, Y. Experimental study on the composite fouling characteristics of calcium carbonate and nanometer magnesia. *J. Mech. Sci. Technol.* **2018**, *32*, 497–504. [CrossRef]
3. Pourabdollah, K. Fouling formation and under deposit corrosion of boiler firetubes. *J. Environ. Chem. Eng.* **2021**, *9*, 104552. [CrossRef]

4. Awais, M.; Bhuiyan, A.A. Recent advancements in impedance of fouling resistance and particulate depositions in heat ex-changers. *Int. J. Heat. Mass Transf.* **2019**, *141*, 580–603. [CrossRef]
5. Giannetti, N.; Yamaguchi, S.; Saito, K.; Tanaka, K.; Ogami, H. A cost effective and non-intrusive method for performance pre-diction of air conditioners under fouling and leakage effect. *Sustain. Energy Technol. Assess.* **2020**, *42*, 100856.
6. Xu, Z.; Zhao, Y.; He, J.; Qu, H.; Wang, Y.; Wang, B. Fouling characterization of calcium carbonate on heat transfer surfaces with sodium carboxymethyl cellulose as an inhibitor. *Int. J. Therm. Sci.* **2021**, *162*, 106790. [CrossRef]
7. Zhao, Y.; Xu, Z.; Wang, B.; He, J. Scale inhibition performance of sodium carboxymethyl cellulose on heat transfer surface at various temperatures: Experiments and molecular dynamics simulation. *Int. J. Heat Mass Transf.* **2019**, *141*, 457–463. [CrossRef]
8. Khormali, A.; Koochi, M.R.; Varfolomeev, M.A.; Ahmadi, S. Experimental study of the low salinity water injection process in the presence of scale inhibitor and various nanoparticles. *J. Pet. Explor. Prod. Technol.* **2022**, *42*, 1118–1126. [CrossRef]
9. Liu, Y.; Wang, J.; Xu, Y.; Wu, B. A deep desalination and anti-scaling electrodeionization (EDI) process for high purity water preparation. *Desalination* **2019**, *468*, 114075. [CrossRef]
10. Zhang, Y.; Cao, S.; Wang, Y.; Wang, G.; Sun, T. Application of alternating electric field scale inhibition device in heat exchange station. *Int. J. Heat Mass Transf.* **2022**, *185*, 122321. [CrossRef]
11. Miller, R.H.B.; Hu, S.; Weamie, S.J.Y.; Naame, S.A.; Kiazolu, D.G. Superhydrophobic Coating Fabrication for Metal Protection Based on Electrodeposition Application: A Review. *J. Mater. Sci. Chem. Eng.* **2021**, *09*, 68–104. [CrossRef]
12. Liu, Y.; Li, Z.; Li, G.; Tang, L. Friction and wear behavior of Ni-based alloy coatings with different amount of WC–TiC ceramic particles. *J. Mater. Sci.* **2023**, *58*, 1116–1126. [CrossRef]
13. Lee, H.; Dellatore, S.M.; Miller, W.M.; Messersmith, P.B. Mussel-Inspired Surface Chemistry for Multifunctional Coatings. *Science* **2007**, *318*, 426–430. [CrossRef] [PubMed]
14. Elmi, F.; Gharakhani, A.; Ghasemi, S.; Alinezhad, H. Self-assemble l-glycine and l-cysteine/polydopamine nanohybrid films coated on 304 stainless steel for corrosion study in sterile seawater. *Prog. Org. Coat.* **2018**, *119*, 127–137. [CrossRef]
15. Park, C.; Lei, J.; Kim, J.-O. Mitigation of biofouling with co-deposition of polydopamine and curcumin on the surface of a thin-film composite membrane. *Chemosphere* **2023**, *310*, 136910. [CrossRef]
16. Zhang, P.; Liu, W.; Rajabzadeh, S.; Jia, Y.; Shen, Q.; Fang, C.; Kato, N.; Matsuyama, H. Modification of PVDF hollow fiber membrane by co-deposition of PDA/MPC-co-AEMA for membrane distillation application with anti-fouling and anti-scaling properties. *J. Membr. Sci.* **2021**, *636*, 119596. [CrossRef]
17. Zhang, L.; Takagi, R.; Wang, S.; Lin, Y.; Guan, K.; Cheng, L.; Matsuyama, H. In situ formation of ultrathin polyampholyte layer on porous polyketone membrane via a one-step dopamine co-deposition strategy for oil/water separation with ultralow fouling. *J. Membr. Sci.* **2021**, *619*, 118789. [CrossRef]
18. Wang, B.B.; Quan, Y.H.; Xu, Z.M.; Zhao, Q. Preparation of highly effective antibacterial coating with polydopa-mine/chitosan/silver nanoparticles via simple immersion. *Prog. Org. Coat.* **2020**, *149*, 105967. [CrossRef]
19. Wang, Z.X.; Yang, H.C.; He, F.; Peng, S.Q.; Li, Y.X.; Shao, L.; Darling, S.B. Mussel-inspired surface engineering for wa-ter-remediation materials. *Matter* **2019**, *1*, 115–155. [CrossRef]
20. Lyu, Q.; Hsueh, N.; Chai, C.L.L. The Chemistry of Bioinspired Catechol(amine)-Based Coatings. *ACS Biomater. Sci. Eng.* **2019**, *5*, 2708–2724. [CrossRef]
21. Ryu, J.H.; Messersmith, P.B.; Lee, H. Polydopamine Surface Chemistry: A Decade of Discovery. *ACS Appl. Mater. Interfaces* **2018**, *10*, 7523–7540. [CrossRef] [PubMed]
22. Yan, Z.S.; Zhang, Y.H.; Yang, H.Y.; Fan, G.D.; Ding, A.; Liang, H.; Li, G.B.; Ren, N.Q.; Bruggen, B. Mussel-inspired polydopa-mine modification of polymeric membranes for the application of water and wastewater treatment: A review. *Chem. Eng. Res. Des.* **2020**, *157*, 195–214. [CrossRef]
23. Wang, X.; Wang, B.-B.; Yang, W.; Zhao, Q.; Xu, Z.-M.; Yan, W.-M. Fabrication of stable and versatile superhydrophobic PTFE coating by simple electrodeposition on metal surface. *Prog. Org. Coat.* **2022**, *172*, 107090. [CrossRef]
24. Darband, G.B.; Aliofkhazraei, M.; Khorsand, S.; Sokhanvar, S.; Kaboli, A. Science and Engineering of Superhydrophobic Surfaces: Review of Corrosion Resistance, Chemical and Mechanical Stability. *Arab. J. Chem.* **2020**, *13*, 1763–1802. [CrossRef]
25. Liu, E.; Wang, L.; Yin, X.; Hu, J.; Yu, S.; Zhao, Y.; Xiong, W. Fabrication of a Robust Superhydrophobic Ni Coating with Micro–Nano Dual-Scale Structures on 316L Stainless Steel. *Adv. Eng. Mater.* **2021**, *23*, 2000913. [CrossRef]
26. Bernsmann, F.; Ball, V.; Addiego, F.; Ponche, A.; Michel, M.; Gracio, J.J.d.A.; Toniazzo, V.; Ruch, D. Dopamine−Melanin Film Deposition Depends on the Used Oxidant and Buffer Solution. *Langmuir* **2011**, *27*, 2819–2825. [CrossRef] [PubMed]
27. Schindler, S.; Bechtold, T. Mechanistic insights into the electrochemical oxidation of dopamine by cyclic voltammetry. *J. Electroanal. Chem.* **2019**, *836*, 94–101. [CrossRef]
28. Xiang, M.S.; Jiang, M.H.Z.; Zhang, Y.Z.; Liu, Y.; Shen, F.; Yang, G.; He, Y.; Wang, L.L.; Zhang, X.H.; Deng, S.H. Fabrication of a novel superhydrophobic and superoleophilic surface by one-step electrodeposition method for continuous oil/water sepa-ration. *Appl. Surf. Sci.* **2018**, *434*, 1015–1020. [CrossRef]
29. Sun, H. COMPASS: An ab Initio Force-Field Optimized for Condensed-Phase ApplicationsOverview with Details on Alkane and Benzene Compounds. *J. Phys. Chem. B* **1998**, *102*, 7338–7364. [CrossRef]
30. Rigby, D.; Sun, H.; Eichinger, B.E. Computer simulations of poly (ethylene oxide): Force field, pvt diagram and cyclization behaviour. *Polym. Int.* **1997**, *44*, 311–330. [CrossRef]

31. Bunte, S.W.; Sun, H. Molecular Modeling of Energetic Materials: The Parameterization and Validation of Nitrate Esters in the COMPASS Force Field. *J. Phys. Chem. B* **2000**, *104*, 2477–2489. [CrossRef]
32. Sun, H.; Ren, P.; Fried, J. The COMPASS force field: Parameterization and validation for phosphazenes. *Comput. Theor. Polym. Sci.* **1998**, *8*, 229–246. [CrossRef]
33. Zhou, H.M.; Chen, R.R.; Liu, Q.; Liu, J.Y.; Yu, J.; Wang, C.; Zhang, M.L.; Liu, P.L.; Wang, J. Fabrication of ZnO/epoxy resin su-perhydrophobic coating on AZ31 magnesium alloy. *Chem. Eng. J.* **2019**, *368*, 261–272. [CrossRef]
34. Stalin, B.; Sudha, G.; Kailasanathan, C.; Ravichandran, M. Effect of MoO_3 ceramic oxide reinforcement particulates on the microstructure and corrosion behaviour of Al alloy composites processed by P/M route. *Mater. Today Commun.* **2020**, *25*, 101655. [CrossRef]
35. Park, I.C.; Kim, S.J. Determination of corrosion protection current density requirement of zinc sacrificial anode for corro-sion protection of AA5083-H321 in seawater. *Appl. Surf. Sci.* **2020**, *509*, 145346. [CrossRef]
36. Dai, W.; Liu, Y.; Huang, N.; Lan, R.; Zheng, K.; Lu, Y.; Li, J.; Jiang, Y.; Sun, Y. Selective corrosion of β-Sn and intermetallic compounds in an Ag–Sn alloy at different potentials in NaCl and Na_2SO_4 solutions. *Corros. Sci.* **2023**, *212*, 110958. [CrossRef]
37. Jiang, D.; Zhou, H.; Wan, S.; Cai, G.-Y.; Dong, Z.-H. Fabrication of superhydrophobic coating on magnesium alloy with improved corrosion resistance by combining micro-arc oxidation and cyclic assembly. *Surf. Coat. Technol.* **2018**, *339*, 155–166. [CrossRef]
38. Ahmadi, S.; Khormali, A.; Khoutoriansky, F.M. Optimization of the demulsification of water-in-heavy crude oil emulsions using response surface methodology. *Fuel* **2022**, *323*, 124270. [CrossRef]
39. Verma, C.; Lgaz, H.; Verma, D.; Ebenso, E.E.; Bahadur, I.; Quraishi, M. Molecular dynamics and Monte Carlo simulations as powerful tools for study of interfacial adsorption behavior of corrosion inhibitors in aqueous phase: A review. *J. Mol. Liq.* **2018**, *260*, 99–120. [CrossRef]
40. Zhao, Y.; Xu, Z.M.; Wang, B.B.; Wang, J.T. The inhibition of sodium carboxymethyl cellulose on calcite growth by molecular dynamics simulation. *Macromol. Theor. Simul.* **2019**, *28*, 1900019. [CrossRef]